



TOPICAL REVIEW

Measuring exciton-phonon coupling in semiconductor nanocrystals

RECEIVED
20 December 2022REVISED
27 March 2023ACCEPTED FOR PUBLICATION
13 June 2023PUBLISHED
5 July 2023Albert Liu^{1,*} , Diogo B Almeida^{2,4} , Steven T Cundiff³  and Lazaro A Padilha^{2,*} ¹ Max Planck Institute for the Structure and Dynamics of Matter, Hamburg, Germany² Instituto de Física ‘Gleb Wataghin’, Universidade Estadual de Campinas, Campinas, São Paulo, Brazil³ Department of Physics, University of Michigan, Ann Arbor, MI, United States of America⁴ Centro de Ciências Naturais e Humanas, Universidade Federal do ABC, Santo André, São Pau, Brazil

* Authors to whom any correspondence should be addressed.

E-mail: albert.liu@mpsd.mpg.de and padilha@ifi.unicamp.br**Keywords:** quantum dots, nonlinear optics, ultrafast spectroscopy, dephasing**Abstract**

At low excitation density, the dynamics of excitons in semiconductor nanocrystals are largely dictated by their interactions with the underlying atomic lattice. This exciton-phonon coupling (EPC) is responsible, for example, for absorption and luminescence linewidths at elevated temperatures, relaxation processes following optical excitation, and even degradation of quantum coherent applications. Characterizing and understanding EPC is therefore central to guiding rational design of colloidal nanocrystal materials and their device applications. In this review, we compare different spectroscopic methods of measuring exciton-phonon interactions and the complementary information that they provide. We emphasize the development of a new technique, termed multidimensional coherent spectroscopy, that circumvents many of the limitations of traditional methods.

1. Introduction

Semiconductor nanocrystals (SNCs) are often referred to as ‘artificial atoms’. This moniker refers to the fact that, in nanocrystals of dimensions comparable to or smaller than the exciton Bohr diameter, quantum confinement due to their small size gives rise to discrete atom-like energy levels. The resulting sharp and size-tunable optical resonances have led SNCs to find applications in numerous areas ranging from photovoltaics [1] to display technologies [2], and even biomedical applications [3].

Despite parallels between the optical properties of SNCs and those of atoms and molecules, important differences arise (primarily) from the extended nuclear structure in SNCs. Perhaps the most obvious difference is the introduction of lattice vibrations (phonons) in SNCs, which interact with electronic excitations just as in bulk semiconductors [4]. This so-called exciton-phonon coupling (EPC) underlies many of the salient optoelectronic properties of SNCs, and is therefore of primary importance to experimentally characterize.

For measuring EPC, a specific set of spectroscopic techniques has been developed and standardized over the past century. By far the most commonly used are absorption/photoluminescence spectroscopy and spontaneous Raman spectroscopy, due to the simple requirement of a continuous-wave light source. Stroboscopic techniques based on pulsed-laser light sources such as pump-probe and photon-echo spectroscopy are also widespread due to their ability to measure coherent dynamics of electronic excitations. In recent years however, a new technique has emerged that circumvents many limitations of the traditional methods mentioned above, namely multidimensional coherent spectroscopy (MDCS) [5, 6]. The unique capabilities of MDCS in regards to measuring EPC will be a primary focus of this review.

This review is organized as follows. We begin by reviewing the basic aspects of EPC in the usual Condon approximation. We then outline one-dimensional characterization techniques, in which the experimental

observable is resolved along one spectral axis. Finally, we introduce the technique of MDCS, and present a selection of exemplary studies on nanocrystals that reveal information uniquely accessible via MDCS in both the time- and frequency-domains.

2. Exciton-Phonon Coupling

In both molecular and condensed materials, the Hamiltonian to describe EPC is often partitioned into an electronic system and a thermal reservoir. The reservoir is usually well-approximated by an ensemble of harmonic oscillators which, to lowest-order, couple linearly to the electronic system. The resultant Hamiltonian is the well-known ‘spin-boson’ Hamiltonian [7]:

$$H = |e\rangle\langle e|\hbar\omega_{eg} + \sum_{\{\alpha\}} \hbar\omega_{\alpha} a_{\alpha}^{\dagger} a_{\alpha} + |e\rangle\langle e| \sum_{\{\alpha\}} \sqrt{s_{\alpha}} (a_{\alpha}^{\dagger} + a_{\alpha}) \quad (1)$$

where $\hbar\omega_{eg}$ is the electronic transition energy, $a_{\alpha} (a_{\alpha}^{\dagger})$ is the annihilation (creation) operator for phonon mode α of resonance frequency $\hbar\omega_{\alpha}$, and s_{α} is the Huang–Rhys factor [8] that quantifies the coupling strength for mode α . In order, each term represents the energy of the electronic excitation, the energy of the thermal reservoir, and the linear coupling strength respectively.

Is this physical picture valid for both molecular vibrations and phonons in solids? In molecular systems, α simply indexes each vibration that couples to the electronic degrees of freedom. In solids however, α indexes not only the individual phonon modes, but also their associated continuum of wavevectors. An additional integral over phonon wavevector is therefore introduced in the Hamiltonian (1) for each summation, and the coupling strength s_{α} likewise becomes a momentum-dependent quantity. We may therefore transition between the two cases of molecular vibrations and phonons in solids by considering either a discrete ensemble of coupled harmonic oscillators or a continuum of modes with an energy dispersion in momentum.

To aid intuition, we may revert the phonon modes into classical harmonic oscillators of coordinates q_{α} . Focusing on the effect of the coupling term in the electronic excited state $|e\rangle$, such linear coupling does not change the resonance frequency of the phonon modes but will shift its potential minimum coordinate. The effective potentials resulting from a single phonon mode may be depicted by the ubiquitous ‘displaced oscillator’ diagram shown in figure 1.

This diagram emphasizes the Born–Oppenheimer approximation that was implicitly made in our discussion, in which the electronic potential energies become parametric functions of a given vibrational coordinate q_{α} . Note that each displaced oscillator describes the energy dependence of only a single mode α , and the full potential energy surface shares the dimensionality of all modes $\{\alpha\}$. In the case of molecular vibrations or a weakly-dispersive phonon mode with well-defined energy, the optical properties of the system may therefore be described by transitions between two manifolds of energy levels with separate electronic and vibrational contributions. The following discussions of this review will be framed in this perspective.

3. One-dimensional characterization techniques

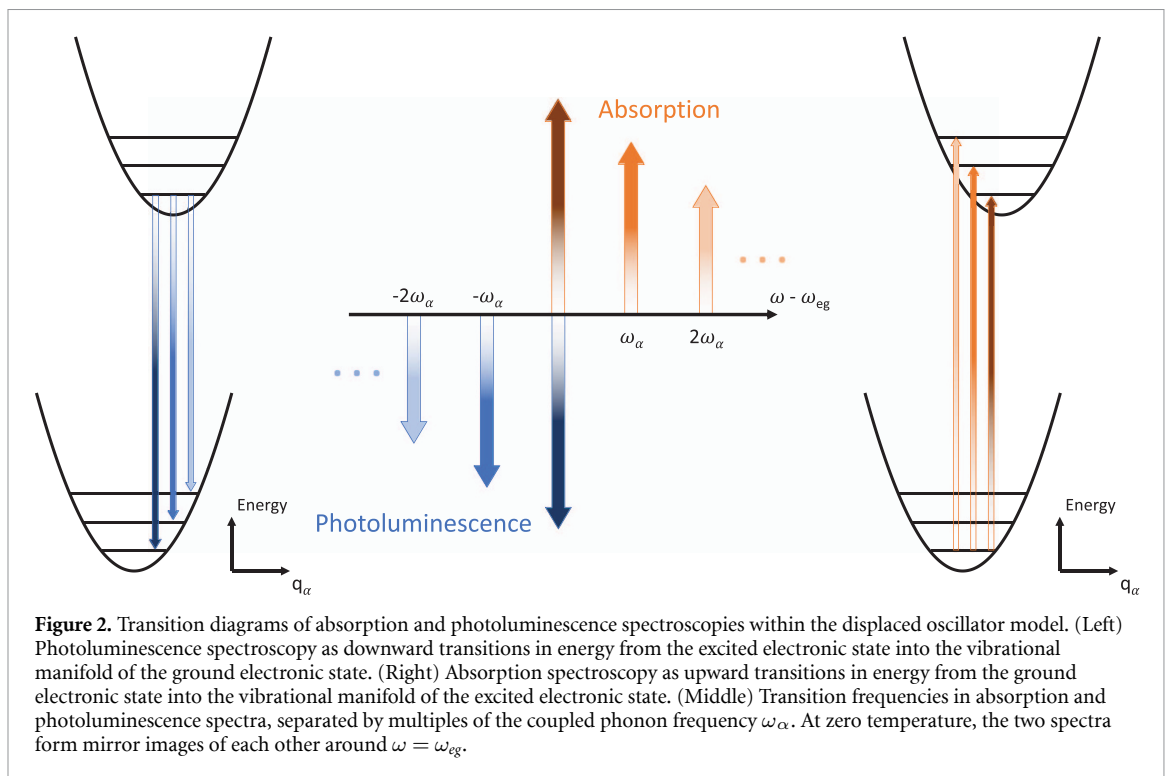
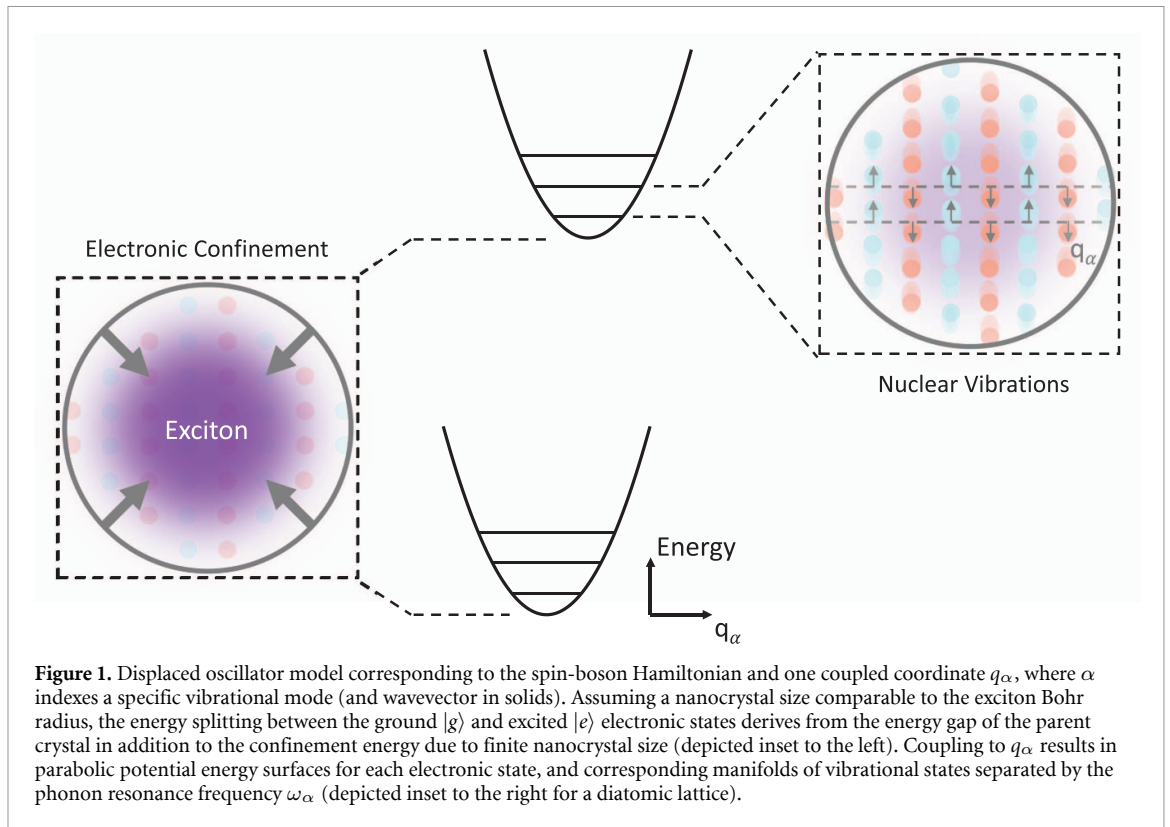
The most common type of technique for characterizing EPC are so-called one-dimensional spectroscopies, in which an experimental observable \mathcal{O} is resolved along a single frequency axis. Though \mathcal{O} may be general, we limit the observables considered here to emitted ‘signal’ electric fields E_{sig} . To compare these various techniques and their interpretations in a unified fashion, it is useful to consider the specific scaling of E_{sig} with excitation field E_{exc} :

$$E_{\text{sig}} \propto \chi^{(n)} E_{\text{exc}}^n \quad (2)$$

where $\chi^{(n)}$ is the optical susceptibility that governs the strength of an optical response. In the language of nonlinear optics, n is referred to as the order of an underlying light–matter interaction, and allows us to interpret each experiment as n optical transitions within the displaced oscillator model shown in figure 1.

3.1. Absorption and photoluminescence spectroscopy

Perhaps the two most common and conceptually simplest techniques are absorption/photoluminescence spectroscopy [9]. The observables for each technique are optical absorption and emission resolved as a function of the frequencies of the incident and emitted light, respectively. As linear ($n = 1$) spectroscopies, each process may be interpreted as a single optical transition within the displaced oscillator model, shown in figure 2.



In the absorption diagram on the right of figure 2, a (in principle infinite) series of upward transitions to states within the vibrational manifold of $|e\rangle$ are shown, with increasing transition frequencies separated by multiples of the phonon frequency ω_α . A corresponding photoluminescence diagram is shown on the left of figure 2 with a series of downward transitions into the vibrational manifold of $|g\rangle$. In contrast to optical absorption, the photoluminescence transition frequencies decrease by multiples of ω_α and forms a mirror image of the absorption spectrum (shown in the middle of figure 2).

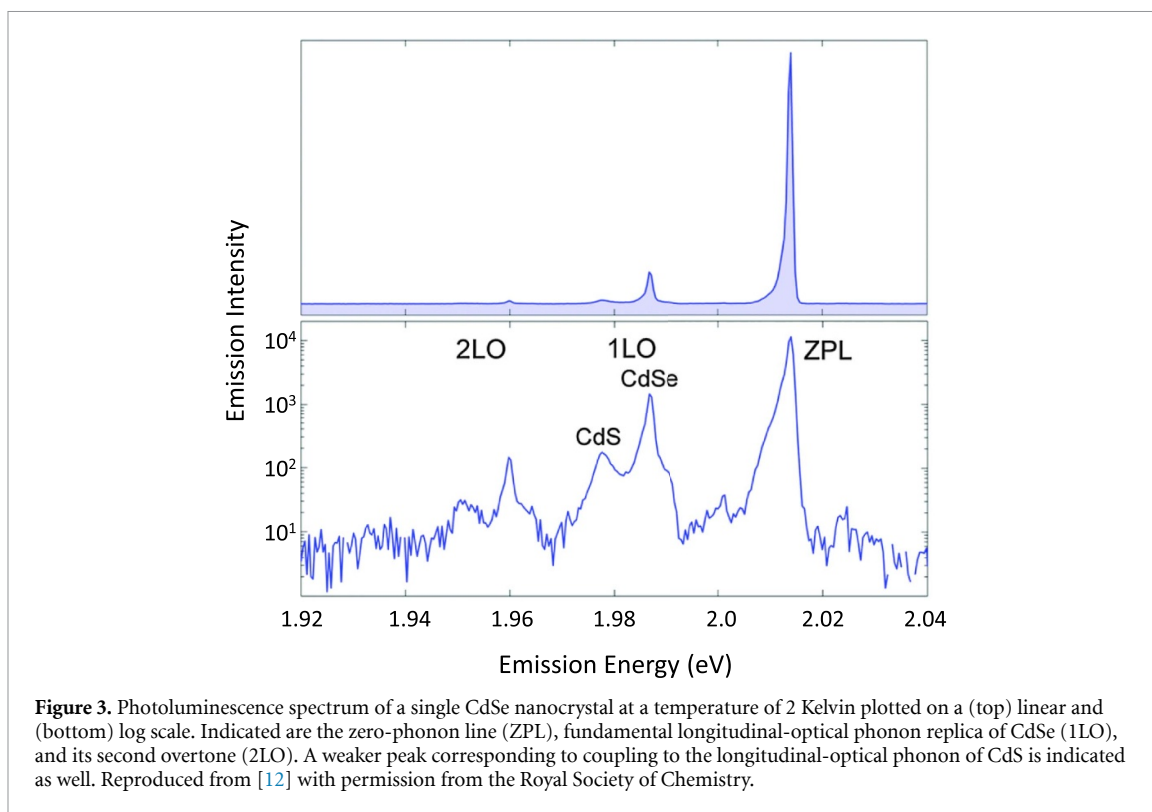


Figure 3. Photoluminescence spectrum of a single CdSe nanocrystal at a temperature of 2 Kelvin plotted on a (top) linear and (bottom) log scale. Indicated are the zero-phonon line (ZPL), fundamental longitudinal-optical phonon replica of CdSe (1LO), and its second overtone (2LO). A weaker peak corresponding to coupling to the longitudinal-optical phonon of CdS is indicated as well. Reproduced from [12] with permission from the Royal Society of Chemistry.

Two assumptions are made in the diagrams of figure 2, namely that (1) optical absorption occurs primarily from the vibrational ground state of $|g\rangle$ and that (2) luminescence following photoexcitation occurs after relaxation to the vibrational ground state of $|e\rangle$. These assumptions are usually satisfied when the Boltzmann energy $k_B T$ is small compared to the phonon energy $\hbar\omega_\alpha$, and thus, at elevated temperatures additional transitions from vibrational excited states must be considered.

In real systems, various factors may complicate the measurement of clean phonon replicas as depicted in figure 2. For example, increasing temperature is always accompanied by thermal broadening of resonance lineshapes. If the transition linewidth becomes comparable to a given phonon energy, observation of phonon replicas is no longer possible. In SNCs, a more problematic issue is inhomogeneous broadening of the exciton resonance [10]. Variations in nanocrystal shape and size of an ensemble translate into variations of exciton resonance energy, resulting in static broadening of resonance linewidths. The primary way of overcoming this limitation has been via single-nanocrystal spectroscopies [11], in which ensemble disorder is circumvented completely at the expense of experimental difficulty, signal strength, and particle statistics. An exemplary single-nanocrystal photoluminescence spectrum of CdSe nanocrystals reported by Fernée *et al* is shown in figure 3, in which two phonon replicas from the longitudinal-optical phonon mode of CdSe are observed [12].

Even in inhomogeneously-broadened ensembles, EPC may be inferred indirectly from variations in optical properties with temperature [13]. In particular, the existence of EPC shifts the exciton resonance energy by an amount proportional to the phonon mode occupation, a temperature dependent quantity. This shift is not necessarily linear, nor monotonic as shown in figure 4 by Liu *et al* for the case of CsPbI₃ nanocrystals. A fit to the temperature dependence reveals both the resonance frequencies of the coupled phonon modes as well as their relative coupling strengths [14]. Similar signatures may be observed in renormalization of the photoluminescence center energy [15], though care should be taken in considering the additional effect of temperature-dependent Stokes-shifts of origins other than EPC.

3.2. Raman spectroscopy

Another popular technique for characterization of EPC is spontaneous Raman spectroscopy [16], in which light of frequencies ω_{in} impinges on a material and subsequently scatters into optical modes of frequencies $\omega_{out} = \omega_{in} \pm \omega_\alpha$, where ω_α is the frequency of the scattered Raman mode [17].

In general, two types of scattering processes are possible, namely elastic (Rayleigh) scattering and inelastic (Raman and Brillouin) scattering. At zero temperature, excited vibrational modes are unoccupied

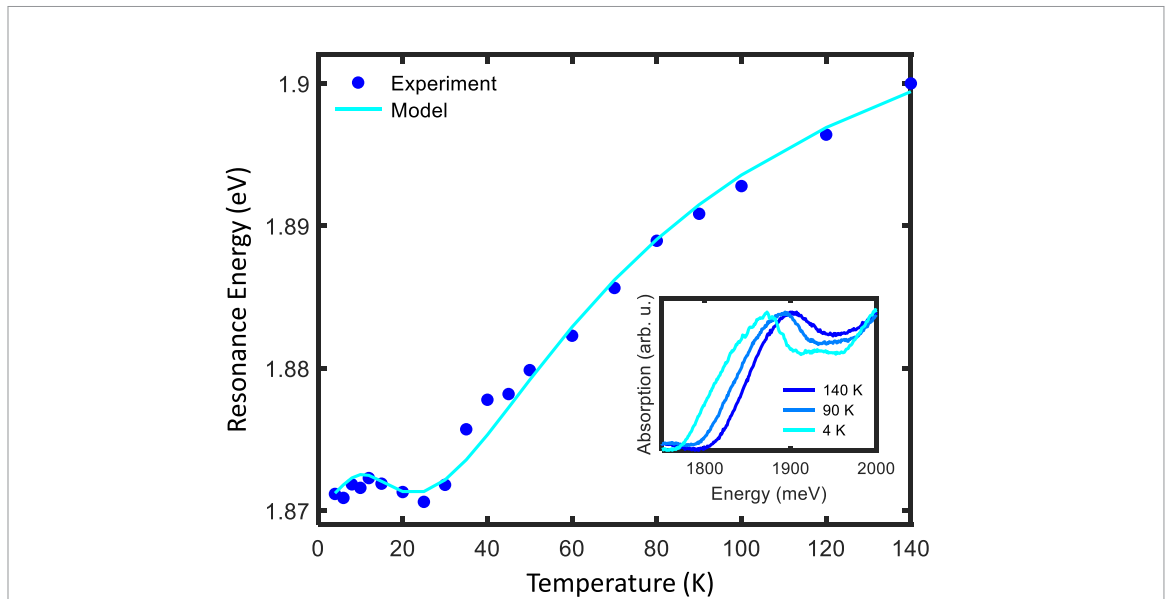


Figure 4. Center energies of the lowest exciton absorption resonance in CsPbI₃ nanocrystals as a function of temperature are plotted as blue dots. The non-monotonic temperature dependence requires coupling to at least three vibrational modes, and a fit to the data by a three-oscillator model is plotted as the light-blue line. Representative absorption spectra at three temperatures are plotted inset. Reprinted from [14], with the permission of AIP Publishing.

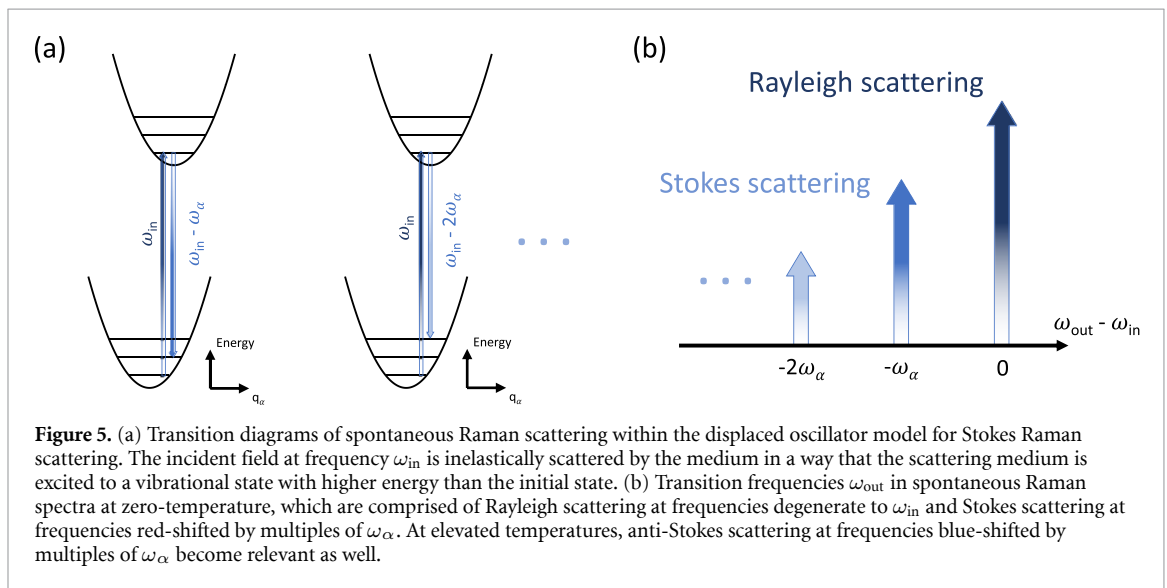
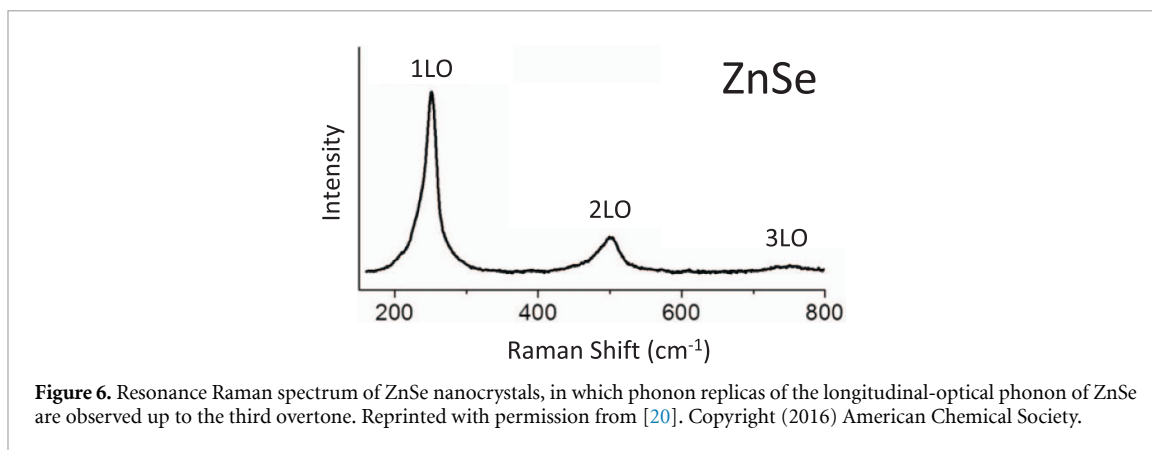


Figure 5. (a) Transition diagrams of spontaneous Raman scattering within the displaced oscillator model for Stokes Raman scattering. The incident field at frequency ω_{in} is inelastically scattered by the medium in a way that the scattering medium is excited to a vibrational state with higher energy than the initial state. (b) Transition frequencies ω_{out} in spontaneous Raman spectra at zero-temperature, which are comprised of Rayleigh scattering at frequencies degenerate to ω_{in} and Stokes scattering at frequencies red-shifted by multiples of ω_{α} . At elevated temperatures, anti-Stokes scattering at frequencies blue-shifted by multiples of ω_{α} become relevant as well.

and inelastic scattering may only occur through creation of vibrational excitations. This process in which the scattered light is redshifted ($\omega_{in} > \omega_{out}$) is known as Stokes scattering, and is depicted in figure 5. The inverse anti-Stokes scattering process ($\omega_{in} < \omega_{out}$) becomes relevant at elevated temperatures and is not shown here. It should be noted that the incident photon energies $\hbar\omega_{in}$ are conventionally chosen to be lower than any electronic resonances.

Two considerations make spontaneous Raman spectroscopy difficult to implement experimentally. First, the Raman scattering probability is limited by occupation of the relevant vacuum photon mode, rendering spontaneous Raman signals orders of magnitude weaker than incident fields. Depending on the application, incident field strengths may also be limited due to confounding effects of interband background signals and sample heating. Second, inferring EPC from spontaneous Raman spectra requires spectral separation of (anti-)Stokes scattering fields from the incident fields. Care must therefore be taken in spectral filtering of the incident field to avoid overlap of the incident spectrum and vibrational sidebands, a requirement that becomes more stringent with decreasing vibrational energy. With these limitations in mind, we highlight below three variations of Raman spectroscopy that have proven relevant for SNCs.



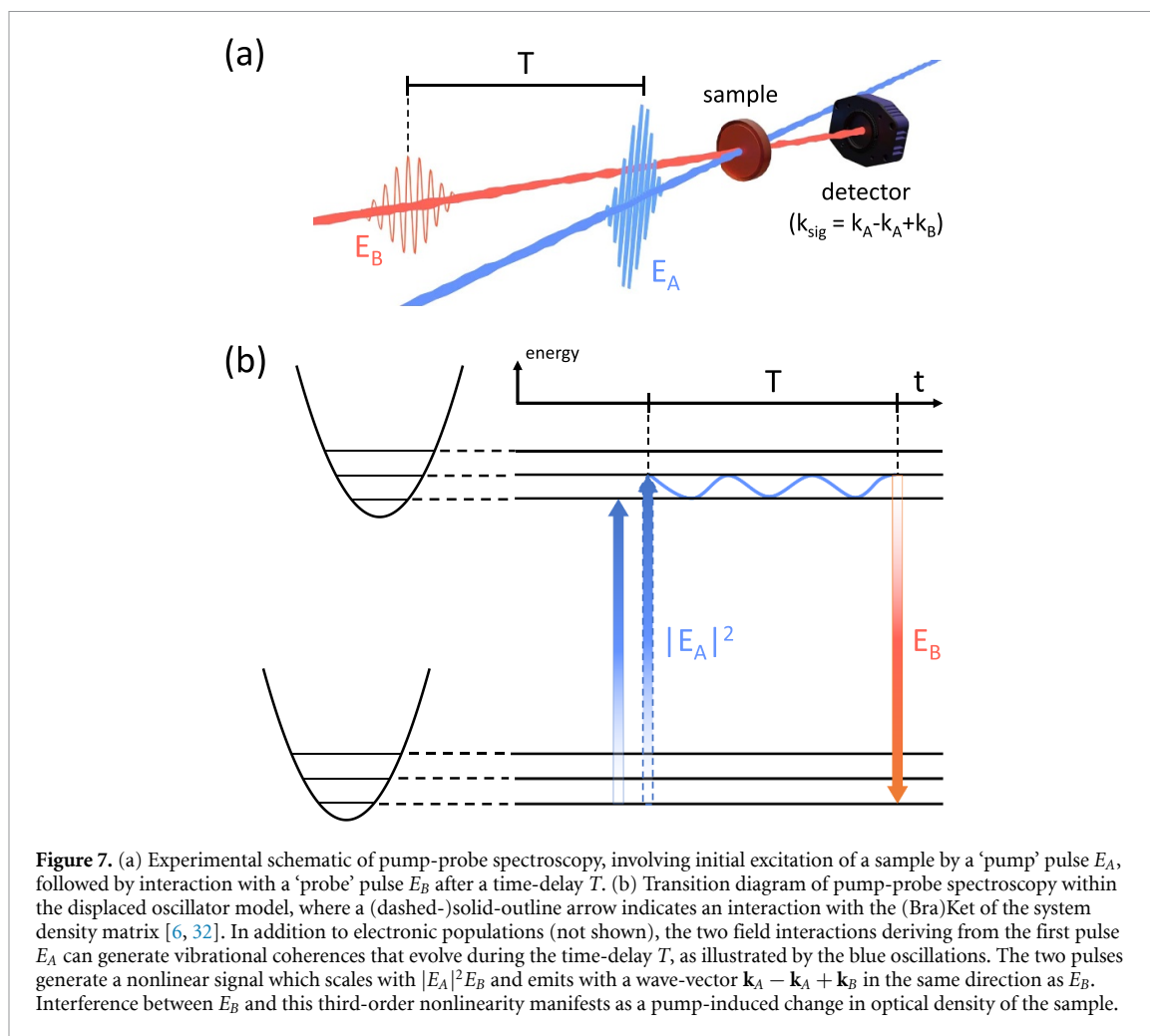
If incident photon energies are tuned into resonance with an electronic transition the Raman scattering cross-sections of phonon modes are greatly increased. This situation is known as ‘resonance Raman scattering’ [18], and a resonance Raman spectrum of ZnSe nanocrystals reported by Gong *et al* (where the second and third overtones of the ZnSe longitudinal-optical phonon are visible) is shown in figure 6. This technique enables the observation of higher-order Raman overtones, and from the intensity ratios between a Raman scattering peak and its overtones, it is possible to extract a Huang–Rhys factor for the EPC [19]. Unfortunately, simple expressions exist only under strict assumptions concerning the coupled electronic state(s), reducing the generality of such analyses.

Another powerful method to enhance weak Raman scattering signals is via plasmon-enhanced Raman spectroscopy [21], otherwise known by its more specific variants termed surface-enhanced Raman spectroscopy (SERS) [22] and tip-enhanced Raman spectroscopy (TERS) [23]. In general, SERS involves the excitation of samples in proximity to a metallic object or environment, resulting in signal increase reaching orders of magnitude. This enhancement has been attributed to both concomitant excitation of resonant surface plasmon modes that generate significant enhancement of local fields [24] as well as chemical interactions between the sample and surface [25]. Of course a concomitant increase in experimental complexity is unavoidable, with SERS requiring more sophisticated sample and substrate preparation as well as optical microscopy. Spatial resolution may be additionally achieved with TERS, in which a scanning probe microscope is used to focus the plasmon-enhanced field with sub-nm resolution. We note that with the advantages of TERS, experimental requirements also become more stringent with the requirement of an ultra-high vacuum sample environment.

Lastly we discuss perhaps the most versatile method of Raman signal enhancement, termed coherent Raman spectroscopy. In contrast to spontaneous Raman spectroscopy, in which the light scattering process is induced by a vacuum photon mode, coherent Raman spectroscopy involves a stimulated scattering process by an additional driving laser [26]. In addition to a scattering efficiency increase by orders of magnitude, the scattered light is also rendered coherent by the additional external field. Of the variants of coherent Raman spectroscopy, so-called coherent anti-Stokes Raman scattering (CARS) [27] is arguably the most commonly used for SNCs. CARS exploits a nonlinear process in which the additional field interaction generates an intermediate vibrational excitation in the electronic ground-state, leading to stimulated anti-Stokes scattering. A primary reason for its widespread adoption is that the detected anti-Stokes scattering fields are blue-shifted in frequency with respect to background fluorescence. Furthermore, in contrast to the other Raman spectroscopy techniques described above, CARS is usually performed with pulsed laser sources with sufficient bandwidth to stimulate anti-Stokes scattering. The use of short pulses of light to stimulate vibrational excitations motivates a more general class of *time-resolved* nonlinear optical spectroscopies that probe dynamic signatures of EPC in time, the focus of the following section.

3.3. Time-resolved four-wave mixing spectroscopies

We have so far discussed absorption/photoluminescence spectroscopy and Raman spectroscopy variations, techniques that relate generally EPC to changes of optical properties in the frequency-domain. However, the development of pulsed lasers enabled measurement of EPC *dynamics* in the time-domain on their intrinsic time-scales as well. As conjugate variables, optical responses in time- and frequency- contain identical information concerning exciton-phonon interactions. However, time-resolved spectroscopic methods offer various advantages over their frequency-domain counterparts.

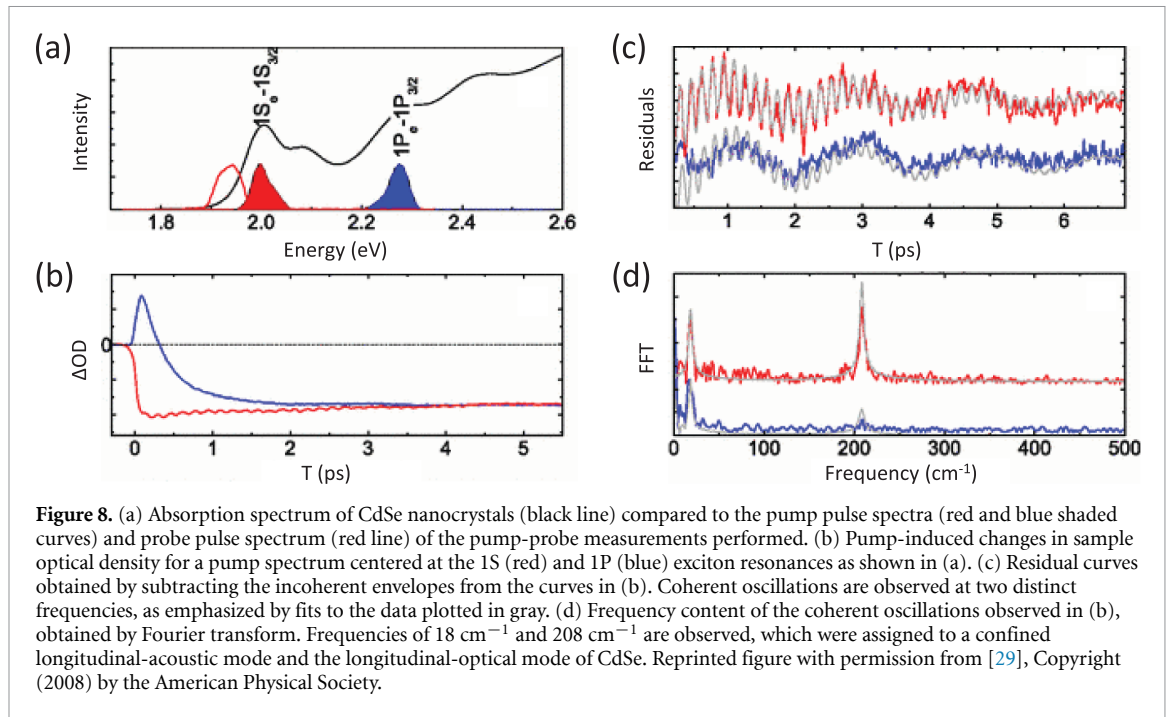


For example, energy relaxation and dissipation become far more intuitive and easily quantified in the time-domain as decay curves (compared to subtle deviation of spectral lineshapes from ideal Lorentzians in the frequency-domain). Perhaps less obvious is the advantage gained from compressing the electromagnetic energy of a light source into a short window in time. That is, one finds dramatically higher peak electric fields for pulsed lasers over continuous-wave lasers with equivalent time-averaged power. Nonlinear optical responses therefore become readily accessible with pulsed excitation, and in this section we focus on two examples of time-resolved four-wave mixing ($n = 3$) spectroscopies [28], pump-probe and photon-echo spectroscopy, towards studying EPC in SNCs.

3.3.1. Pump-probe spectroscopy

Perhaps the most well-known example of time-resolved spectroscopy is pump-probe spectroscopy, which involves the excitation of a material with two pulses of light with a controllable time-delay. An initial ‘pump’ field E_A excites the material into a non-equilibrium state, after which a second ‘probe’ field E_B interrogates any change in optical properties induced by the pump pulse. In the context of SNCs the optical property measured by the probe pulse is usually optical density, measured by a change in transmission through a sample. This variation of pump-probe spectroscopy is also known as transient absorption spectroscopy, and is depicted schematically in figure 7(a).

From a more general perspective, transient absorption spectroscopy measures a third-order nonlinearity which scales with $|E_A|^2 E_B$ and emits with a wavevector $\mathbf{k}_A - \mathbf{k}_A + \mathbf{k}_B$. The two initial field interactions $|E_A|^2$ create either a population state or a vibrational coherence that evolves at the phonon eigenfrequency ω_α . The latter possibility is plotted in figure 7(b), which depicts the evolution of vibrational coherence in the excited electronic state potential. After a time delay T , the incident probe pulse encounters a modulated optical density proportional to the instantaneous vibrational coordinate. Experimental transient absorption measurements reported by Sagar *et al* [29] are shown in figures 8(a) and (b), in which the pump spectrum



was tuned to two distinct exciton transitions in CdSe SNCs. In addition to incoherent relaxation dynamics, coherent oscillations are observed as a function of the pump-probe time-delay T , which become apparent in the residual time traces in figure 8(c) upon subtraction of the incoherent envelopes. Their Fourier spectra in figure 8(d) identify two coupled phonon modes as a confined longitudinal-acoustic mode ($\omega_\alpha \approx 18\text{ cm}^{-1}$) and the longitudinal-optical mode of CdSe ($\omega_\alpha \approx 208\text{ cm}^{-1}$), where EPC to the latter mode is suppressed for the upper 1P exciton state.

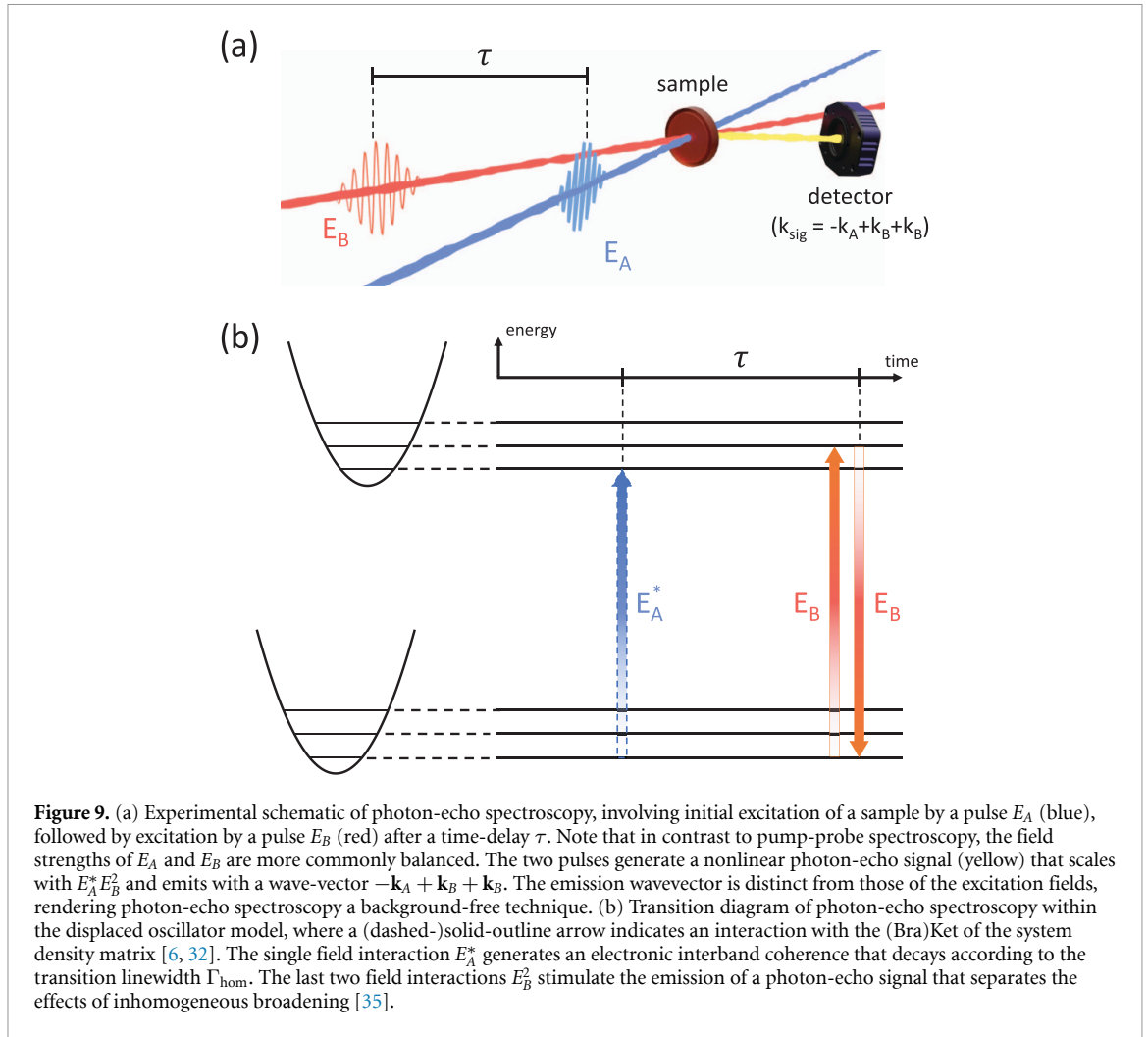
We note that pump-probe measurements are also sensitive to vibrational modes beyond those of the host lattice. Confined vibrational modes arising from the finite nanocrystal geometry may also result in coherent modulation of the probe field, as reported by Lin *et al* in gold nanocrystals [30]. More sophisticated ‘pump-pump-probe’ experiments have also been reported, for example by Spann *et al* in CdTe_{1-x}Se_x nanocrystals [31], in which coherent control of the phonon modulation was achieved by splitting a single pump pulse into a pair with variable inter-pulse time-delay. Such three-pulse experiments resemble the more general technique of multidimensional spectroscopy, which comprise the focus of the last part of this review.

3.3.2. Photon-echo spectroscopy

Another powerful four-wave mixing technique is photon-echo spectroscopy [17, 28], which involves detection of an optical analogue to spin-echoes [33] in nuclear magnetic resonance. Photon echoes may be generated by the same excitation configuration shown in figure 7(a) with an emission wavevector $-\mathbf{k}_A + \mathbf{k}_B + \mathbf{k}_B$, rendering photon-echo spectroscopy a background-free technique as shown in figure 9(a). As indicated by the emission wavevector, the photon echo signal scales with $E_A^* E_B^2$ (where E_A^* is the conjugate of the complex field amplitude E_A). The first excitation pulse creates an electronic coherence as shown in figure 9(b), which evolves for a time delay τ until photon echo emission is produced by the second excitation pulse via E_B^2 .

The utility of photon-echo spectroscopy is apparent in ensembles with an inhomogeneous distribution of resonance energies, as shown in figure 10(a). While the inhomogeneous linewidth Γ_{inhom} normally obscures the homogeneous linewidth Γ_{hom} in other techniques, photon-echo spectroscopy separates the two broadening mechanisms in the time-domain such that the photon-echo signal decays with a lifetime $1/\Gamma_{\text{hom}}$ that is averaged over the ensemble [34]. The lifetime corresponding to the inhomogeneous linewidth $1/\Gamma_{\text{inhom}}$ then manifests in the temporal width of the photon-echo pulse that is emitted a time τ after the last interaction with pulse E_B [35].

As a recent example, Bohn *et al* have performed photon echo measurements on methylammonium lead iodide nanoplatelets to measure the ensemble-averaged homogeneous linewidth as a function of temperature, which exhibit thermal line-broadening due to EPC. By fitting the temperature dependence to a one-mode model, coupling to a longitudinal-optical mode of energy $E_{\text{LO}} = 21 \pm 3\text{ meV}$ was inferred. Similar

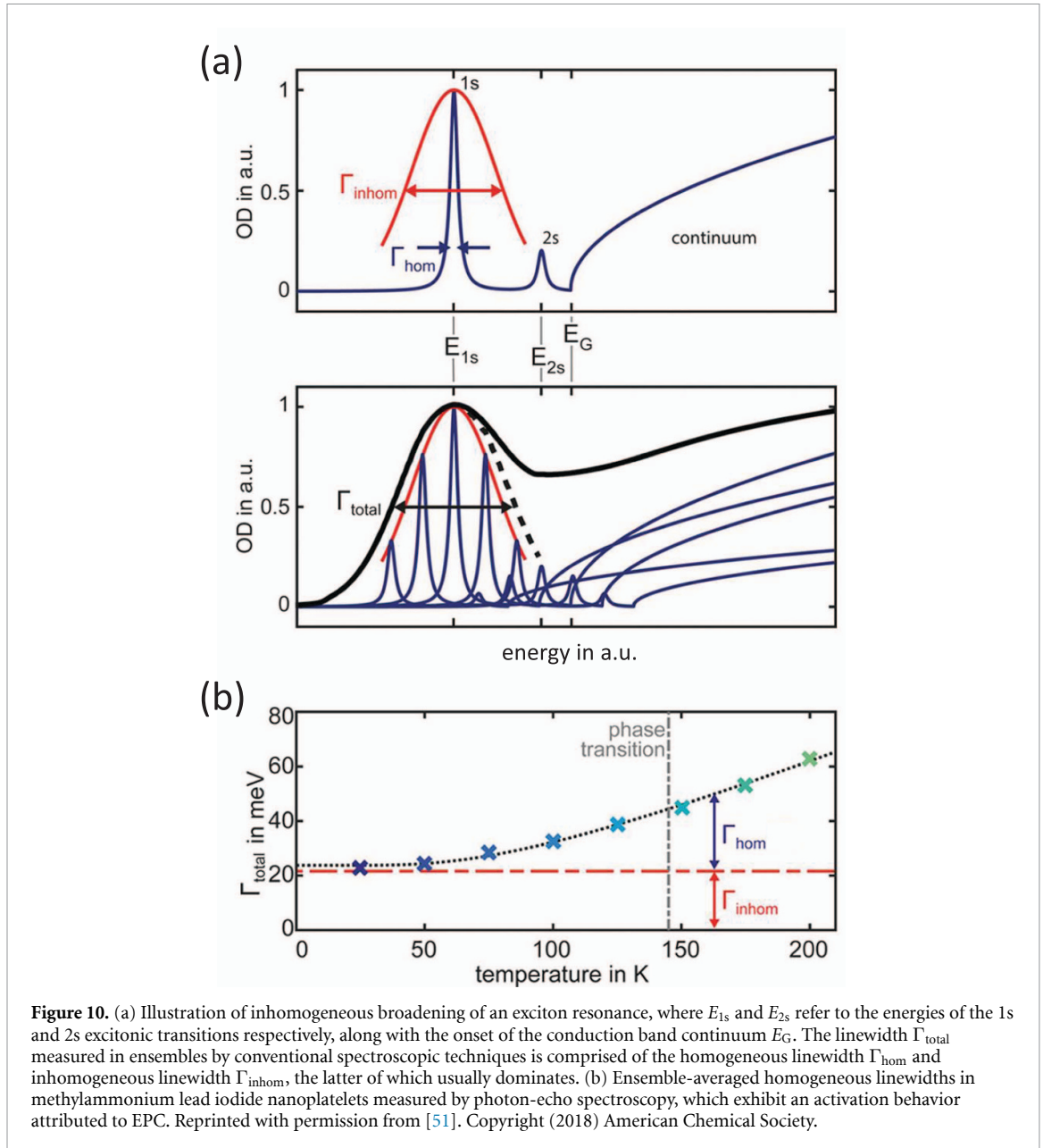


measurements have also been performed on other nanocrystal systems, for example PbS [36], CdSe [34, 37], and CsPbBr₂Cl [38] SNCs.

4. MultiDimensional Coherent Spectroscopy

Despite their utility, most nonlinear spectroscopic techniques (including pump-probe spectroscopy and photon-echo spectroscopy) measure either only a portion or a projection of the full complex, multi-dimensional optical susceptibility $\chi^{(n)}$ [39]. These piece-wise measurements of $\chi^{(n)}$ discard salient information about the underlying dynamics while also introducing ambiguities in interpretation. In recent years, a technique capable of measuring the entire complex nonlinear optical response has been developed, known as MDCS [5]. MDCS is an extension of sophisticated Fourier transform spectroscopies, originally developed for nuclear magnetic resonance, to optical frequencies, and has emerged as the preeminent method for disentangling complex dynamics in a wide range of materials ranging from molecules [40, 41] to semiconductors [42, 43], and even biological systems [44, 45].

In its most general realization, MDCS involves excitation of a sample with three excitation pulses which cooperatively stimulate the emission of a nonlinear optical signal. This signal may be isolated either [46] via wavevector phase-matching [47] as considered here or other frequency-domain methods [48]. Usually a photon-echo signal is chosen to be measured, which is emitted with a wavevector $-\mathbf{k}_A + \mathbf{k}_B + \mathbf{k}_C$ as shown in figure 11(a) with the time-ordering shown in figure 11(b). The distinguishing characteristic of MDCS is that the temporal dynamics of the photon-echo signal during the three time delays $\{\tau, T, t\}$ are Fourier transformed to correlate their frequency-domain responses in a multi-dimensional spectrum. The time-delays τ and T must therefore be stable to within a small fraction of the oscillation period of interband coherences, a technical challenge that requires active stabilization of path lengths [47], passively-stable pulse



generation methods [49], or active monitoring of path-length fluctuations [50]. We will defer further discussion of experimental implementations [49] and the microscopic dynamics underlying various nonlinear optical signals to more detailed [17, 32, 39], and focus on exemplary MDCS studies that revealed unique aspects of EPC in SNCs in the remainder of this review.

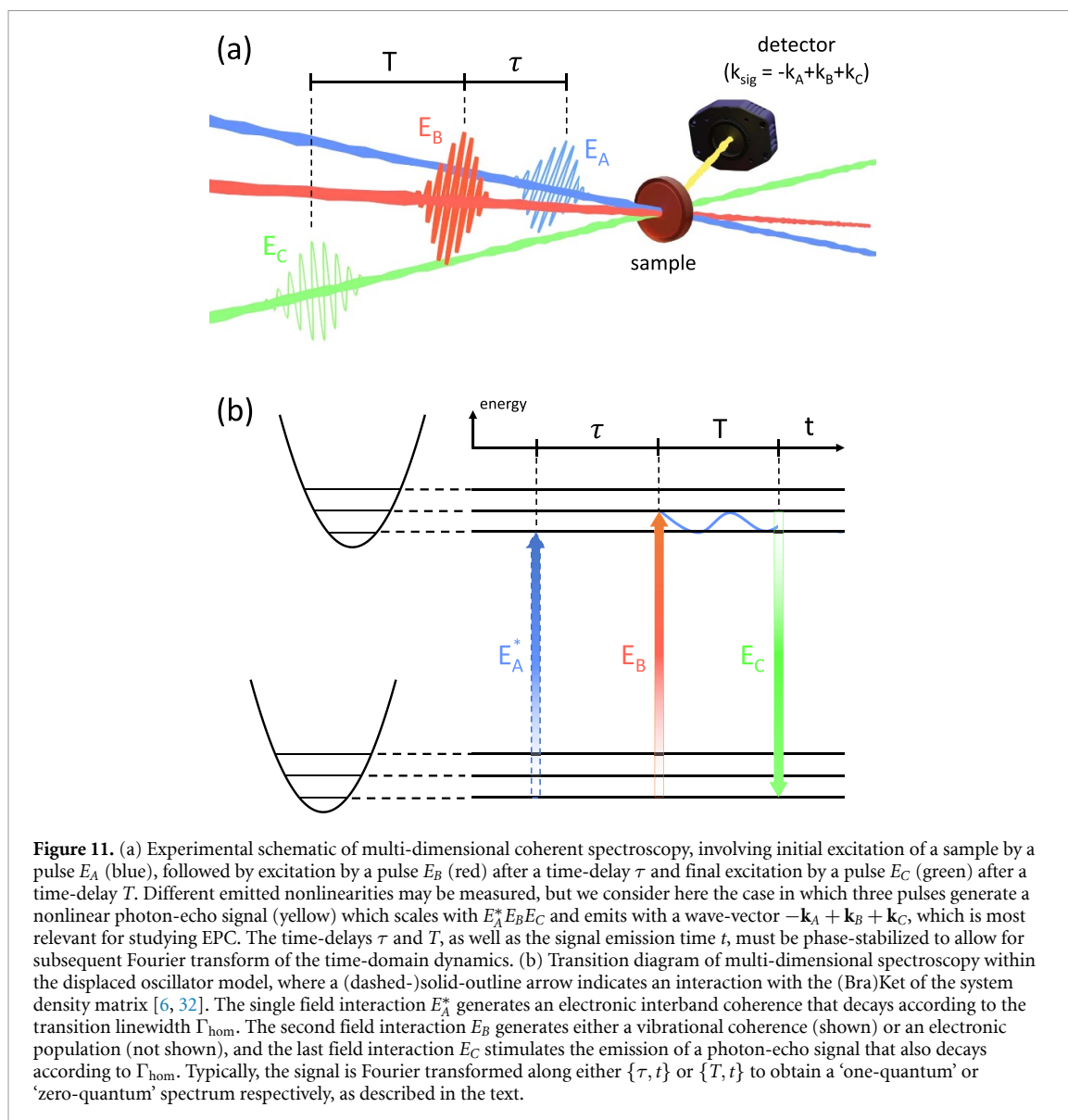
4.1. Spectral signatures of EPC in 2D spectra

Perhaps the most powerful capability of MDCS is to project homogeneous and inhomogeneous broadening mechanisms into orthogonal directions in a ‘one-quantum spectrum’ [35], which correlates absorption and emission dynamics of a material via Fourier transform along the two time axes $\{\tau, t\}$ in figure 11(b). In this way, homogeneous lineshapes may be directly resolved in an inhomogeneously-broadened nanocrystal ensemble without isolating single emitters [52].

Counter-intuitively, the homogeneous linewidth of the zero-phonon line directly informs EPC in nanocrystals. The zero-phonon linewidth γ , which reflects spectral broadening due to elastic exciton-phonon scattering, scales with temperature T , according to the expression:

$$\gamma(T_s) = \gamma_0 + AT_s + \frac{B}{e^{E_{\text{ph}}/k_B T_s} - 1} \quad (3)$$

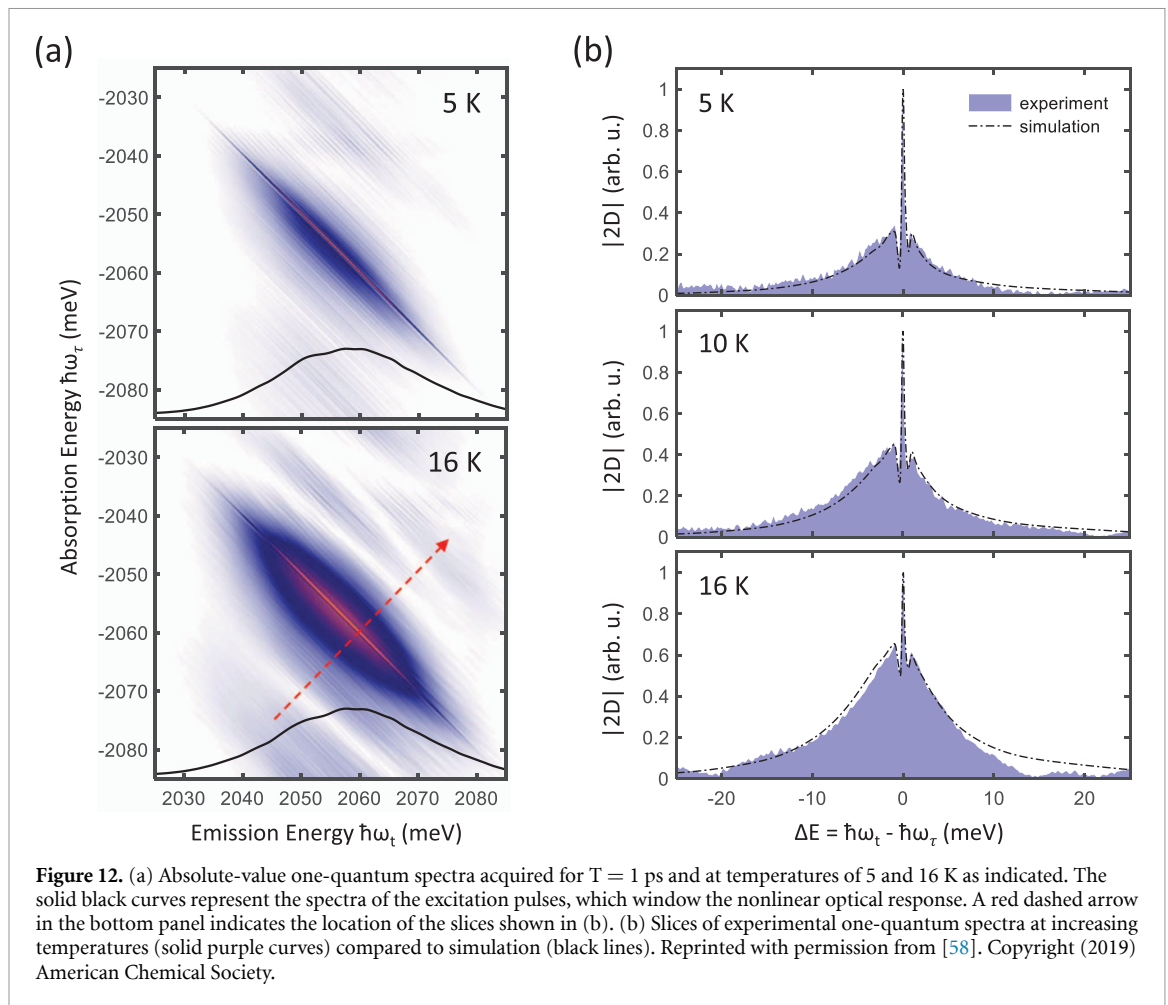
where γ_0 is the intrinsic linewidth limited by population relaxation, the second linear dependence on temperature reflects broadening due to an acoustic phonon continuum, and the last term reflects broadening



due to a phonons of discrete energy E_{ph} . The EPC strengths A and B , as well as the relevant phonon energies E_{ph} , may therefore be characterized by measuring the temperature dependence of a zero-phonon linewidth [53]. Two such experiments have been reported recently by Yu *et al* in CsPbBr₃ nanocubes [54] and Liu *et al* in CsPbI₃ nanoplatelets [55], which both observed broadening due to the acoustic phonon continuum primarily.

For low temperatures at which dephasing times in SNCs become comparable to characteristic frequencies of the coupled thermal environment, the homogeneous lineshape contains information about the frequency-dependent structure (spectral density) [56] of the system-bath coupling. However, the non-Lorentzian lineshapes that reflect these physics have proven difficult to resolve using single-nanocrystal spectroscopies due to signal strength limitations and variation between individual emitters of an ensemble [57].

To overcome these limitations, Liu *et al* applied MDCS to CdSe SNCs and resolved their ensemble-averaged homogeneous linewidths as a function of temperature [58]. As shown in figure 12(a), non-Lorentzian lineshapes were observed in the one-quantum spectra that strongly depended on temperature. By examining slices along the direction of homogeneous broadening in figure 12(b), a narrow peak and broad pedestal were identified as the zero-phonon line and EPC to the acoustic phonon continuum respectively. While the matched sound velocities between CdSe and the surrounding glass matrix sustained delocalized acoustic vibrations, the finite nanocrystal size also introduced confined torsional vibrations of discrete energies [4]. The lineshape was then reproduced by simulating simultaneous coupling to both confined and delocalized vibrational modes, emphasizing the power of MDCS to characterize spectral densities in complex quantum systems.

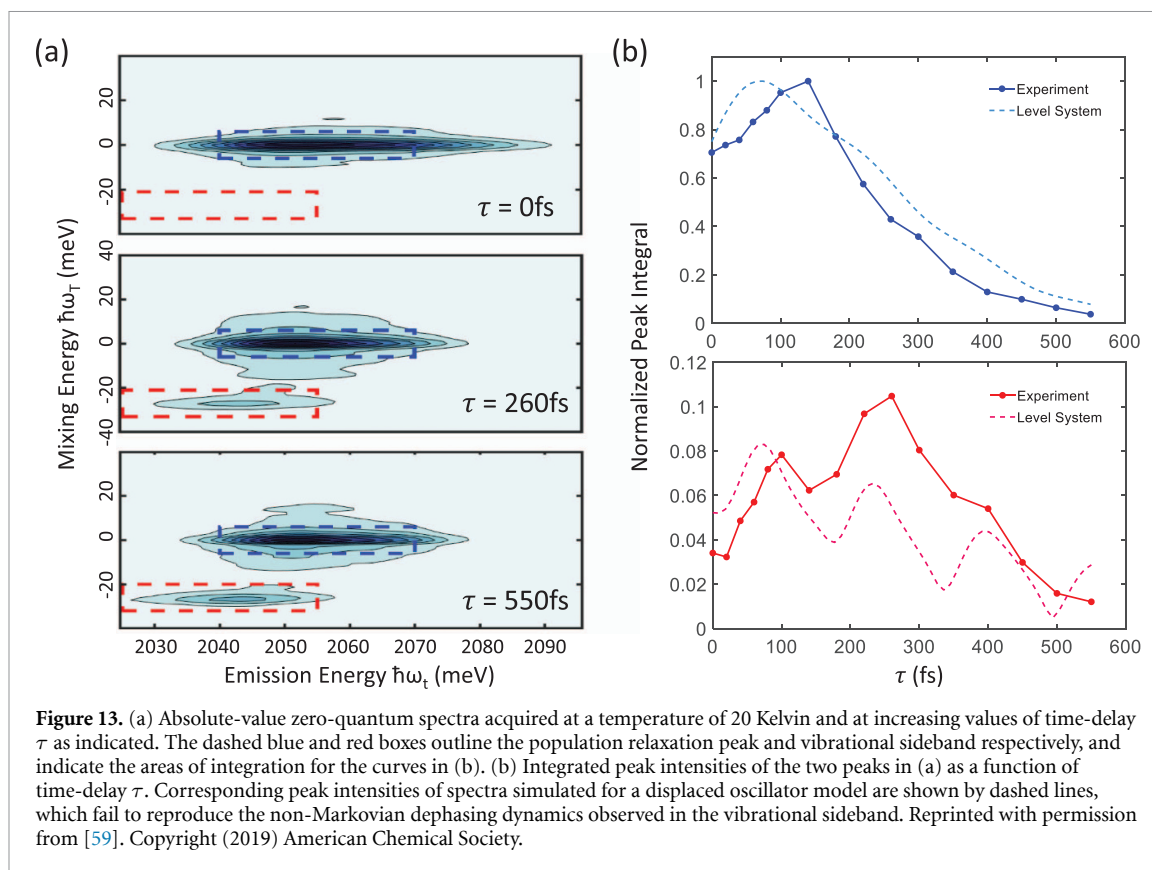


4.2. Time-domain signatures of EPC in 2D spectra

In the previous section one-quantum spectra exhibiting strongly non-Lorentzian spectral lineshapes, arising from EPC to low-energy acoustic modes, were presented as a window into the microscopic system-bath interactions. Spectral lineshapes may be thought of as the frequency-domain counterpart to time-domain dephasing of optical coherences, and non-Lorentzian lineshapes may therefore be related to deviations from exponential dephasing. From a microscopic perspective, non-exponential dephasing indicates a finite correlation time of the underlying energy-gap fluctuations [17], or in other words a violation of the usual Markovian approximation. Coupling to optical phonon modes may also induce non-exponential dephasing in principle, but such signatures are even more difficult to measure due to a more limited phonon density of states and confounding influence of the acoustic phonon bath.

Frequency-domain techniques such as photoluminescence and Raman spectroscopies are capable of measuring EPC strengths and associated vibrational resonance frequencies, though quantifying subtle deviations from Lorentzian lineshapes of vibrational sidebands has proven impractical. On the other hand, time-domain techniques such as pump-probe and photon-echo spectroscopies primarily measure either vibrational dephasing dynamics or zero-phonon line dephasing [60] respectively. The limitations of such one-dimensional techniques may be circumvented by MDCS in a mixed time- and frequency-domain approach. Specifically, a ‘zero-quantum spectrum’ [61] correlates vibrational and emission dynamics via Fourier transform along the time axes $\{T, t\}$ in figure 11(b). The remaining time delay τ then provides access to dephasing dynamics of the initial optical coherences.

Such zero-quantum spectra of CdSe CNCs were reported by Liu *et al* [59] and shown in figure 13(a), in which two peaks are observed that separate population relaxation (blue box) and vibrational (red box) dynamics. By observing the evolution of each peak intensity as a function of delay τ , dephasing dynamics of the exciton transition are resolved with respect to the involvement of a coupled optical vibration. The evolution of the population relaxation peak plotted in the top of figure 13(a) is well-reproduced by the conventional Kubo ansatz for the correlation function of the energy gap dynamics [32], which assumes Gaussian fluctuations with a finite correlation time, while the evolution of the vibrational sideband plotted



in the bottom of figure 13(b) deviates from simulation. Indeed, these vibrationally-induced non-Markovian dephasing dynamics were revealed only after distilling vibrationally-coupled interband coherences by MDCS.

Another notable study concerning temporal signatures of EPC was reported by Seiler *et al* [62], in which the homogeneous linewidth resolved in one-quantum spectra was further measured as a function of the intermediate time-delay T . In this way, modulation of the homogeneous linewidth due to variation in vibrational amplitude may be resolved directly in time. Exemplary CdSe and CsPbI₃ SNCs were studied to reveal contrasting behavior of the lineshape dynamics, namely reversible modulation due to coherent phonon dynamics in covalently-bonded CdSe and diffusive dynamics due to polaron formation in ionic-bonded CsPbI₃. Further quantitative analysis allowed for extraction of the polaron formation time and reorganization energy in CsPbI₃ SNCs.

5. Summary and outlook

EPC plays an important role in the fundamental properties and many practical applications of SNCs. Yet compared to our knowledge of electronic structure in SNCs, our understanding of EPC in these systems remains limited. From our perspective, experimental measurements can inform design principles and constrain theoretical models, and are essential to advancing our understanding in this area. We have therefore reviewed common techniques for characterizing EPC in SNCs, and have also introduced multi-dimensional spectroscopy as a powerful new method to circumvent many limitations of traditional techniques [43]. These are summarized in table 1.

Many interesting aspects of EPC in SNCs remain open for investigation, in particular with MDCS, and we give three examples of particular interest to us. First, characterizing the spectral density of EPC for more complicated unit cells than the simple case of CdSe [58], for example in perovskite nanocrystals [43], would be useful in relation to their unique optoelectronic properties. We have also observed the importance of dimensionality in ‘freezing out’ coupling to various vibrational modes [14, 55, 63], and further investigation of the dimensional cross-over would be useful for understanding the underlying mechanisms. Finally, we mention the aspect of EPC in various colloidal heterostructures. By varying the band-alignment of constituent interfaces, electrons and holes can be localized in either the same, or different spatial regions of SNCs. Unique heterostructure geometries, such as so-called colloidal nanoshells [64], also offer the possibility to engineer the exciton wavefunction in new ways. The effects of both band-alignment and heterostructure geometry on EPC remain attractive frontiers to explore.

Table 1. Summary of techniques for characterizing exciton-phonon coupling in semiconductor nanocrystals. Light source requirements and experimental observables are listed.

Technique	Light Source ^a	Experimental Observables for EPC
Absorption	BB	Temperature dependence (exciton resonance energy)
Photoluminescence	NB/BB	Temperature dependence (exciton resonance energy)
Raman	NB	Phonon sideband to overtone intensity ratio
Pump-Probe	BB,TR	Amplitude/phase modulation of coherent oscillations
Photon-Echo	BB,TR	Temperature dependence (exciton homogeneous linewidth)
MDCS	BB,TR	Homogeneous spectral lineshape, time-domain dephasing

^a NB = Narrowband, BB = Broadband, TR = Time-Resolved.

Data availability statement

No new data were created or analysed in this study.

Acknowledgments

Albert Liu was supported by a fellowship from the Alexander von Humboldt Foundation; Diogo B Almeida and Lazaro A Padilha thank the support from São Paulo State funding agency, FAPESP grants 2019/22576-8 and 2018/15574 respectively.

ORCID iDs

Albert Liu  <https://orcid.org/0000-0001-6718-3719>

Diogo B Almeida  <https://orcid.org/0000-0003-2369-4618>

Steven T Cundiff  <https://orcid.org/0000-0002-7119-5197>

Lazaro A Padilha  <https://orcid.org/0000-0002-8825-6611>

References

- [1] Kirmani A R, Luther J M, Abolhasani M and Amassian A 2020 *ACS Energy Lett.* **5** 3069
- [2] Liu Z *et al* 2020 *Light Sci. Appl.* **9** 83
- [3] Wagner A M, Knipe J M, Orive G and Peppas N A 2019 *Acta Biomater.* **94** 44
- [4] Takagahara T 1996 *J. Lumin.* **70** 129
- [5] Cundiff S T and Mukamel S 2013 *Phys. Today* **66** 44
- [6] Li H, Lomsadze B, Moody G, Smallwood C and Cundiff S 2023 *Optical Multidimensional Coherent Spectroscopy* (Oxford: Oxford University Press)
- [7] Leggett A J, Chakravarty S, Dorsey A T, Fisher M P A, Garg A and Zwerger W 1987 *Rev. Mod. Phys.* **59** 1–85
- [8] de Jong M, Seijo L, Meijerink A and Rabouw F T 2015 *Phys. Chem. Chem. Phys.* **17** 16959
- [9] Fox M 2010 *Optical Properties of Solids* (Oxford: Oxford University Press)
- [10] Empedocles S A, Norris D J and Bawendi M G 1996 *Phys. Rev. Lett.* **77** 3873
- [11] Fernée M J, Tamarat P and Lounis B 2014 *Chem. Soc. Rev.* **43** 1311
- [12] Fernée M J, Sinito C, Mulvaney P, Tamarat P and Lounis B 2014 *Phys. Chem. Chem. Phys.* **16** 16957
- [13] Cardona M 2005 *Solid State Commun.* **133** 3
- [14] Liu A, Bonato L G, Sessa F, Almeida D B, Isele E, Nagamine G, Zagonel L F, Nogueira A F, Padilha L A and Cundiff S T 2019 *J. Chem. Phys.* **151** 191103
- [15] Saran R, Heuer-Jungemann A, Kanaras A G and Curry R J 2017 *Adv. Opt. Mater.* **5** 1700231
- [16] Jones R R, Hooper D C, Zhang L, Wolverson D and Valev V K 2019 *Nanoscale Res. Lett.* **14** 231
- [17] Mukamel S 1999 *Principles of Nonlinear Optical Spectroscopy* (Oxford: Oxford University Press)
- [18] Czernuszewicz R S and Zaczek M B 2011 *Resonance Raman Spectroscopy (Encyclopedia of Inorganic and Bioinorganic Chemistry)* (Chichester: Wiley)
- [19] Kelley A M 2013 *J. Phys. Chem. A* **117** 6143
- [20] Gong K, Kelley D F and Kelley A M 2016 *J. Phys. Chem. C* **120** 29533
- [21] Wang X, Huang S-C, Hu S, Yan S and Ren B 2020 *Nat. Rev. Phys.* **2** 253
- [22] Han X X, Rodriguez R S, Haynes C L, Ozaki Y and Zhao B 2022 *Nat. Rev. Methods Primers* **1** 87
- [23] Verma P 2017 *Chem. Rev.* **117** 6447
- [24] Ding S-Y, Yi J, Li J-F, Ren B, Wu D-Y, Panneerselvam R and Tian Z-Q 2016 *Nat. Rev. Mater.* **1** 16021
- [25] Le Ru E C and Etchegoin P G 2013 *MRS Bull.* **38** 631
- [26] Prince R C, Frontiera R R and Potma E O 2017 *Chem. Rev.* **117** 5070
- [27] Cheng J-X and Xie X S 2004 *J. Phys. Chem. B* **108** 827
- [28] Cho M, Scherer N F, Fleming G R and Mukamel S 1992 *J. Chem. Phys.* **96** 5618
- [29] Sagar D M, Cooney R R, Sewall S L, Dias E A, Barsan M M, Butler I S and Kambhampati P 2008 *Phys. Rev. B* **77** 235321
- [30] Lin K-H, Cheng H-Y, Yang C-Y, Li H-W, Chang C-W and Chu S-W 2018 *App. Phys. Lett.* **113** 171906
- [31] Spann B T and Xu X 2014 *Appl. Phys. Lett.* **105** 083111
- [32] Hamm P and Zanni M 2010 *Concepts and Methods of 2D Infrared Spectroscopy* (Cambridge: Cambridge University Press)
- [33] Hahn E L 1950 *Phys. Rev.* **80** 580

- [34] Mittleman D M, Schoenlein R W, Shiang J J, Colvin V L, Alivisatos A P and Shank C V 1994 *Phys. Rev. B* **49** 14435
- [35] Siemens M E, Moody G, Li H, Bristow A D and Cundiff S T 2010 *Opt. Express* **18** 17699
- [36] Masia F, Langbein W, Moreels I, Hens Z and Borri P 2011 *Phys. Rev. B* **83** 201309
- [37] Masia F, Accanto N, Langbein W and Borri P 2012 *Phys. Rev. Lett.* **108** 087401
- [38] Becker M A, Scarpelli L, Nedelcu G, Rainò G, Masia F, Borri P, Stöferle T, Kovalenko M V, Langbein W and Mahrt R F 2018 *Nano Lett.* **18** 7546
- [39] Liu A and Cundiff S T 2020 *Phys. Rev. Mater.* **4** 055202
- [40] Ginsberg N S, Cheng Y-C and Fleming G R 2009 *Acc. Chem. Res.* **42** 1352
- [41] Le Sueur A L, Horness R E and Thielges M C 2015 *Analyst* **140** 4336
- [42] Cundiff S T, Zhang T, Bristow A D, Karaiskaj D and Dai X 2009 *Acc. Chem. Res.* **42** 1423
- [43] Liu A, Almeida D B, Padilha L A and Cundiff S T 2022 *J. Phys. Mater.* **5** 021002
- [44] Hunt N T 2009 *Chem. Soc. Rev.* **38** 1837
- [45] Petti M K, Lomont J P, Maj M and Zanni M T 2018 *J. Phys. Chem. B* **122** 1771
- [46] Nardin G, Autry T M, Moody G, Singh R, Li H and Cundiff S T 2015 *J. Appl. Phys.* **117** 112804
- [47] Bristow A D, Karaiskaj D, Dai X, Zhang T, Carlsson C, Hagen K R, Jimenez R and Cundiff S T 2009 *Rev. Sci. Instrum.* **80** 073108
- [48] Nardin G, Autry T M, Silverman K L and Cundiff S T 2013 *Opt. Express* **21** 28617
- [49] Fuller F D and Ogilvie J P 2015 *Ann Rev. Phys. Chem.* **66** 667
- [50] Autry T M, Moody G, Fraser J, McDonald C, Mirin R P and Silverman K 2019 *Optica* **6** 735
- [51] Bohn B J, Simon T, Gramlich M, Richter A F, Polavarapu L, Urban A S and Feldmann J 2018 *ACS Photon.* **5** 648
- [52] Liu A 2022 *Nanomaterials* **12** 801
- [53] Liu A, Cundiff S T, Almeida D B and Ulbricht R 2021 *Mater. Quantum Technol.* **1** 025002
- [54] Yu B, Zhang C, Chen L, Huang X, Qin Z, Wang X and Xiao M 2021 *J. Chem. Phys.* **154** 214502
- [55] Liu A, Nagamine G, Bonato L G, Almeida D B, Zagonel L F, Nogueira A F, Padilha L A and Cundiff S T 2021 *ACS Nano* **15** 6499
- [56] Nitzan A 2006 *Chemical Dynamics in Condensed Phases: Relaxation, Transfer and Reactions in Condensed Molecular Systems* (Oxford: Oxford University Press)
- [57] Fernée M J, Littleton B N, Cooper S, Rubinsztein-Dunlop H, Gómez D E and Mulvaney P 2008 *J. Phys. Chem. C* **112** 1878
- [58] Liu A, Almeida D B, Bae W-K, Padilha L A and Cundiff S T 2019 *J. Chem. Phys. Lett.* **10** 6144
- [59] Liu A, Almeida D B, Bae W K, Padilha L A and Cundiff S T 2019 *Phys. Rev. Lett.* **123** 057403
- [60] Nibbering E T J, Wiersma D A and Duppen K 1991 *Phys. Rev. Lett.* **66** 2464
- [61] Yang L, Zhang T, Bristow A D, Cundiff S T and Mukamel S 2008 *J. Chem. Phys.* **129** 234711
- [62] Seiler H, Palato S, Sonnichsen C, Baker H, Socie E, Strandell D P and Kambhampati P 2019 *Nat. Commun.* **10** 4962
- [63] Liu A, Almeida D B, Bonato L G, Nagamine G, Zagonel L F, Nogueira A F, Padilha L A and Cundiff S T 2021 *Sci. Adv.* **7** eabb3594
- [64] Cassidy J and Zamkov M 2020 *J. Chem. Phys.* **152** 110902